Energy efficient area coverage for an autonomous demining robot

José Prado and Lino Marques

Institute of Systems and Robotics,
University of Coimbra,
3030-290 Coimbra, Portugal.
{jaugusto, lino}@isr.uc.pt

Abstract. This work studies different coverage approaches with a mobile robot equipped with a landmine detecting sensor attached to an actuator arm. Different coverage techniques were experiment in this work and the cost benefit was analyzed in terms of energy consumption. The problem of optimising the combined motion of a mobile platform with an arm was addressed. The feasibility and effectiveness of both algorithms are demonstrated by simulation results for coverage work of target area.

1 Introduction

The demining task is as important as dangerous, and humans are frequently put in risk during the search and de-activation of landmines. Therefore, significant efforts are being made by the scientific community, in order to develop systems able to automatically detect landmines while the users are kept safe. Blast antipersonnel mines include less than 100 g of explosive and very little metal. Due to the simple construction, the mines are mostly very cheap, consequently they were extremely spread. The most common type of installation is underground, therefore they are very difficult to see. Different approaches has been proposed for solving the mine detection problem, for example [1] and [2], which used a set of sensors that vary among metal-detectors, ground penetration radars, cameras, chemical sensors and others, the fusion of some of those sensors was also shown to be effective and to reduce the false positives [3].

Independently of the used set of sensors, the robot must carry this set across an area, while reading the ground in its search of land-mines. This task is called robotic coverage. There are several approaches for coverage in the literature and the selection of the proper approach is highly dependant of the application. For example: The line-sweep approach [4] and the spatial cell diffusion [5] are suitable for open rectangular areas due to the shape created by the trajectory of the robot, another important factor of these approaches is that the robot can starts from a corner or even from out-side the area. The smooth spiral path planning [6] and the squared spiral approach requires that the robot starts or ends at the middle of the area, a constraint that might be critical for some applications, as demmining. Multi-robot coverage algorithms [7] deals with the coordination of several robots to cover an area, to have multiple robots covering an area clearly leads to a faster coverage, however, due to collision avoidance processes the

number of maneuvers is higher than with a single robot, consequently also higher is the energy cost of the entire coverage. Target coordinated area coverage approaches [8] are meant to minimize the trajectory path in order to find a single target.

Hence, although the sensing and detection techniques can still be improved, in this paper we assume that once the sensor is swept over the mine, it detects it. Therefore, we focus on analysing the motion of our robot and its end-effector (which carries the sensor) and how this motion affects the energy-efficiency of different coverage techniques applied to our robot (Fig. 1). This work is a part of the ongoing project TIRAMISU (ISR, Coimbra, Portugal) aimed to develop demining technologies; among robots, sensors and devices that endows the exploration of fields and the location of landmines.

Fig. 1. Robot equipped with mine detecting sensors.

2 Related Work

Covering large areas is a task that is obviously useful for a large number of applications such as cleaning large surfaces, mapping purposes [9], and autonomous mine clearance [10]. In indoor environments, the obstacles are usually walls, furniture and structure of the building, while in outdoor environments there can be trees, rocks, ravines, or none. More specifically, for the demining task, the mines by itself shall be considered a special type of obstacle, that after detection, shall be mapped and avoided. Thus, the real coverage path is the motion of the robot when following a coverage plan combined with the effort to avoid stepping on the mines (obstacle avoidance). When applied to large areas, such effort requires that the robot is operational for long periods of time. Therefore, the interest on using algorithms that can maximize the covered area for a certain amount of energy extant on the robot arises.

3 Energy Consumption

3.1 Robot base

A wheeled robot normally has several motors where each one rotates a wheel. The velocity of the i^{th} wheel is defined as $vi = \rho * \omega_{wi}$, where ρ is the wheel's radius and ω_{wi} is the respective motor's angular velocity. Similarly, the velocity of the arm sweep is given by $v5 = b * \omega_a$, where b is the length of the arm and ω_a is the angular velocity of the arm motor. If we consider that our robot exists in a 2D space, it is possible to represent its velocity by three variables: Vx, Vy, and Ω. The matrix $(Vx, Vy, \Omega)^T$ represents the velocities of the robot (linear and angular). Our robot has a skid-steer configuration, the wheels do not steer, the distance between wheels and the distance between axis are the same. From robot's top view, this configuration makes the center of the four wheels as the corners of a perfect square, inscribed in a circle, where the center of the circle is also the center of the robot. (see Fig. 2). Thus, the four wheels are mounted at distance r from the center of the robot.

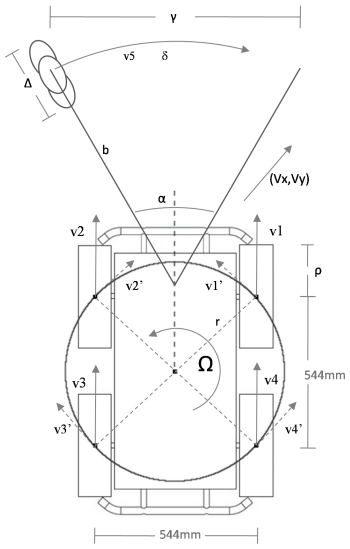

Fig. 2. Kinematics of our robotic platform.

Let $v1$, $v2$, $v3$ and $v4$ be the velocities of the four wheels, and $v5$ the velocity of the arm sweep. Each of the wheels velocity, has a component that potentially performs rotation, this component can be seen as the projection if the velocity vector on the local tangent of the inner circle. Let $v1'$, $v2'$, $v3'$, $v4'$ be the respective potential-rotation components of each wheel velocity, where $vi^2 = vi'^2 + drift^2$. The potential-rotation components will null each other when exist together with the one from the other side of the robot, the same occurs with the drift components, therefore there is no rotation

nor drift when the robot moves strait forward. The relationship between the potential-rotation components of the wheels and the velocity of the robot can be expressed by:

$$\begin{pmatrix} v1' \\ v2' \\ v3' \\ v4' \end{pmatrix} = \begin{pmatrix} \sqrt{\frac{1}{2}} & \sqrt{\frac{1}{2}} & r \\ -\sqrt{\frac{1}{2}} & \sqrt{\frac{1}{2}} & r \\ -\sqrt{\frac{1}{2}} & -\sqrt{\frac{1}{2}} & r \\ \sqrt{\frac{1}{2}} & -\sqrt{\frac{1}{2}} & r \end{pmatrix} \cdot \begin{pmatrix} Vx \\ Vy \\ \Omega \end{pmatrix} \tag{1}$$

This relation, the manipulator Jacobian, allows to control the velocity of the robot $(Vx, Vy, \Omega)^T$ by changing the velocities $(v1, v2, v3, v4)^T$, consequently changing the components $(v1', v2', v3', v4')^T$. Let's consider that $V_t = (Vx_t, Vy_t, \Omega_t)^T$ is the velocity of the robot at time t. The potential-rotation component of the velocity of each wheel at time t is: $vi'(t) = J_{i,1} \cdot Vx(t) + J_{i,2} \cdot Vy(t) + J_{i,3} \cdot \Omega(t)$.

Henceforth, the angular velocities of the respective motors is $\omega_{wi} = \frac{vi(t)}{\rho}$.

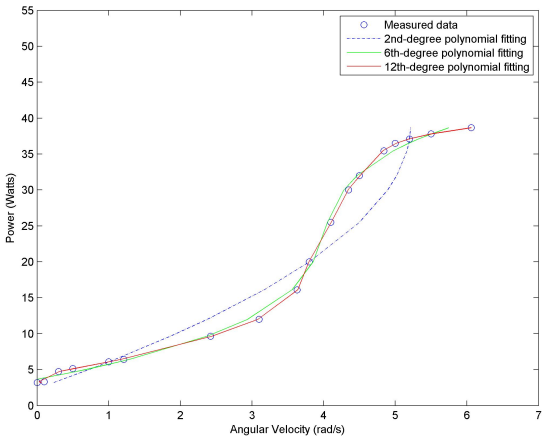

Fig. 3. Power model for different ω.

In order to define the power model, lets consider that $Pm(\omega, \alpha)$ is the consumption of a motor moving at angular velocity ω, and with angular acceleration $\alpha = \frac{d\omega}{dt}$. According to [11], a polynomial fitting is a good approach to model the power of the motors since the behavior of those can be represented by an unbounded function. In [12], the power model of a basic motor was modeled as a second-degree polynomial of ω, in [13] it was shown that a sixth degree model would be more suitable. From our experimental data, see Fig. 3, we find that a 12th-degree polynomial fitting is better than both of the formers. For the 2nd, 6th and 12th degree polynomial fitting, the mean square error respectively decreased from 0.01668, through 0.002720, to 0.000068. The energy consumption per radian is presented in Fig. 4. Notice that for these motors,

an specific interval of angular velocities that lies around the middle velocity, is more energy-efficient. Moreover, once considering that the model presented in Fig. 3 is the power model of the wheels' motors (P_{mw}), in a similar manner we found the power model of the arm motor P_{ma}; thus the power consumption cost function of the robot can be defined as:

$$\sum_{i=1}^{4} P_{mw}(\omega_{wi}, \frac{d\omega_{wi}}{dt}) + P_{ma}(\omega_a, \frac{d\omega_a}{dt}) \tag{2}$$

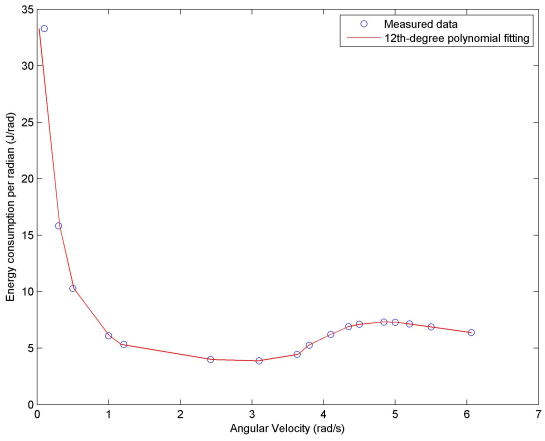

Fig. 4. Energy efficiency of each wheel.

3.2 Robotic arm sweeping

Let α be the maximum angle of the arm sweep, $\frac{\alpha}{2}$ radians to the left and $\frac{\alpha}{2}$ radians to the right. The distance traversed during one arc sweep is $\delta = \alpha \cdot b$. The width of the covered strip is $\gamma = 2\sin(\frac{\alpha}{2})$.

As represented in Fig. 5, let Δ be the size of the sensor, consequently $\frac{\Delta}{2}$ is the distance that the robot shall move forward during one arc sweep. Thus, although setting $\alpha = \pi$ would maximise the coverage area in front of the robot, when moving forward $(0, Vy, 0)^T$, the arm angle of sweeping (α) also affects the maximum velocity of the robot (ω_w), by following relation:

$$\omega_w = \frac{\Delta \cdot \omega_a}{\alpha \cdot \rho} \tag{3}$$

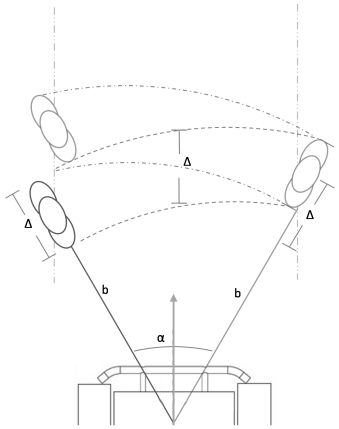

Fig. 5. Combined robotic movement and arm sweeping.

Case Study In our robot, each coil of the metal detector is equipped with one chemical sensor, the arm swiping movement of the arm generates simultaneously 3 lines of dual data. These dual sensor data is fused and interpolated based on the method proposed at [3] and generates an arc strip of covered area in front of the robot with Δ length (see Fig. 5). The size of our dual sensor is $\Delta = 0.62\,m$.

This application bring some constraints to our problem:

- $v5$ is limited to $\frac{1}{2}$ m/s, according to the manual of the metal detector and also with [14], this is the maximum sweep speed accepted for proper sensor functionality;
- according to [15], the size of the robot when rotating over it's own axis is $0.99\,m$;
- the covered strip while the robot moves forward $((0,Vy,0)^T)$ has a detection width of at least $0.99\,m$, for the robot to safely pass through an area without step in mines.
- according to the power model defined on Fig. 3, the optimal speed of the robot would be around 3; to maximize the robot speed the arm angle of sweep need to be as small as possible.

Considering these constraints, and considering that our $b = 1| : m$, the angle of the arm sweep was set to 60 degrees, 30° to the left and 30° to the right. The distance of sweep became $\delta = \frac{\pi b}{3} m$. Thus, the angular velocity of the arm is $\omega_a = \frac{1}{2}$ rad/s. To match the desired scan presented on Fig. 5, without gaps, the robot needs to move $\frac{\Delta}{2} = 0.31\,m$ forward in $\frac{2\pi}{3}$ seconds.

Hence, according to the relation 3, these parameters allows us to apply a maximum angular velocity of the wheels' motors of: $\omega_w = 1.19\,rad/s$, which is inside an acceptable range of energy efficiency for the wheels' motors (see Fig. 4), and it is the optimal configuration that guaranty the arm scan to perform without gaps.

4 Area Coverage

Coverage is the problem of moving a sensor over all points in a given region. Since we already defined the relation between the motion of the sensor and the motion of the robot, we want a energy-efficient path for the robot. Thus, lets make some assumptions about important elements that describe a coverage problem:

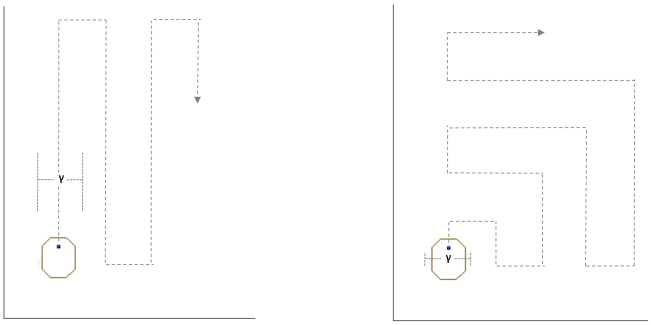

(a) Line-sweep trajectory (b) SCD trajectory

Fig. 6. Target trajectories for both algorithms.

- The coverage region: The region to be covered is continuous and smooth (or can be embedded in the plane), is connected, and is defined by an outer perimeter and some mines (obstacles) in its interior. In this paper we will assume that perimeter is polygonal, and the mines are spread randomly.
- The robot: It is a differential skid steer robot. The starting or ending position of the robot may be specified.
- The sensors: The sensor is considered to be two dimensional and it sweeps through an arc area as the robot moves. The scanned area is larger than the robot.
- The robot can navigate outside the target area in order to maneuver, thus the map is larger than the target area.
- A coverage algorithm must return the coverage path through a detailed sequence of velocities commands for the robot.

As referred in section 2, there are several algorithms for covering a planar area, the selection of the proper approach is highly dependant of the application. As our target application is mine clearance in open fields, some additional constraints take place: the environment is an open out-door area, the robot can not start from the middle/center of the area, the robot shall minimize the number of maneuvers, the area of mine fields are usually polygonal. Considering those constraints, we select two suitable approaches for our analysis, line-sweeping and spatial-cell-diffusion. The energy-efficiency (EE) of a covered rectangular $m \times n$ area, when the robot consumed e energy to cover this area, can be generally defined as: $EE = \frac{m \cdot n}{e}$.

4.1 Line-Sweeping

The line-sweeping (LS) algorithm works in two stages. In the first stage, the algorithm selects the longest edge of the field to determine the optimal direction of the sweep. In the second stage, it generates $\frac{n}{\gamma}$ tracks parallel to the field edges to be used as rows.

Although this algorithm can also be used for unknown sized areas, if the map is giver a priori enhanced decisions can be taken. Thus, let's consider a given rectangular area of size $m \times n$, where $m \geq n$ and γ is the width of the sensor detection area. The number of lines is defined as $\frac{n}{\gamma}$. The LS, described in Algorithm 1, than sends to the navigation cartesian coordinates of the points of rotation, defining the optimal trajectory as represented in Fig. 6(a). Since we are considering that the testing area is strongly connected, a mine field with sparse and randomly distributed mines, this trajectory is achieved without the need of further area segmentation.

Algorithm 1: LS Line-sweeping coverage

Input: Area size= $\{m \times n\}$ Scan strip size= γ
Output: Path=Sequence of navigation points on the map, CmdVel=Sequence of velocities commands
//function path gives the point x, y of the target // given the velocities and distance
if $m > n$ **then**
  $dir \leftarrow m$;
end
else
  $dir \leftarrow n$;
  and robot rotates 90°
end
$tracks \leftarrow \frac{dir}{\gamma}$
for $i \leftarrow 1$ ***to*** $tracks$ **do**
  //Robot moves forward dir distance
  $Path[i] \leftarrow path(f(0,Vy,0)^T, dir)$ $CmdVel[i] \leftarrow navigation(Path[i])$
  $\{v1,v2,v3,v4\} \leftarrow f(0,Vy,0)^T$
  //Robot rotates 90°
  $\{v1,v2,v3,v4\} \leftarrow f(0,0,\Omega)^T$
  //Robot moves forward γ distance
  $Path[i] \leftarrow path(f(0,Vy,0)^T, \gamma)$ $CmdVel[i] \leftarrow navigation(Path[i])$
  $\{v1,v2,v3,v4\} \leftarrow f(0,Vy,0)^T$
  //Robot rotates 90°
  $\{v1,v2,v3,v4\} \leftarrow f(0,0,\Omega)^T$
end
return $Path, CmdVel$

4.2 Spatial Cell Diffusion

The spatial cell diffusion (SCD), described in Algorithm 2, moves the robot in a spiral movement, although it differs from the square-spiral by alternating clock-wise and

counter-clock-wise movements each time robot reaches to a border of the target area. This feature also allows it to be compatible with rectangular areas with $m \neq n$, since the motion starts another spiral when boundaries are reached.

Algorithm 2: SCD Spatial cell diffusion coverage

Input: Area size= $\{m \times n\}$ Scan strip size= γ
Output: Path=Sequence of navigation points on the map, CmdVel=Sequence of velocities commands
//function path gives the point x, y of the target // given the velocities and distance
$tracks \leftarrow \frac{dir}{\gamma}$ bool $side \leftarrow right : side\{right, left\}$ $dist \leftarrow gamma$
//Robot moves forward γ distance
$Path[i] \leftarrow path(f(0,Vy,0)^T, \gamma)$ $CmdVel[i] \leftarrow navigation(Path[i])$
$\{v1, v2, v3, v4\} \leftarrow f(0,Vy,0)^T$ //Robot rotates 90° to the $side$
$\{v1, v2, v3, v4\} \leftarrow f(0,0,\Omega)^T$ **for** $i \leftarrow 1$ ***to*** $tracks$ **do**
  for $j \leftarrow 1$ ***to*** 3 **do**
    if $j \neq 3$ **then**
      //Robot moves forward $dist$ distance
      $Path[i] \leftarrow path(f(0,Vy,0)^T, dist)$ $CmdVel[i] \leftarrow navigation(Path[i])$
      $\{v1, v2, v3, v4\} \leftarrow f(0,Vy,0)^T$
      if $j = 1$ **then**
        //Robot rotates 90°
        $\{v1, v2, v3, v4\} \leftarrow f(0,0,\Omega)^T$
      end
      if $j = 2$ **then**
        $side \leftarrow notside$
        //Invert rotation and rotates 90°
        $\{v1, v2, v3, v4\} \leftarrow f(0,0,\Omega)^T$
      end
    end
    else
      //Robot moves forward γ distance
      $Path[i] \leftarrow path(f(0,Vy,0)^T, \gamma)$ $CmdVel[i] \leftarrow navigation(Path[i])$
      $\{v1, v2, v3, v4\} \leftarrow f(0,Vy,0)^T$
      //Robot rotates 90°
      $\{v1, v2, v3, v4\} \leftarrow f(0,0,\Omega)^T$
    end
  end
end
return $Path, CmdVel$

5 Experimental Tests

5.1 Simulated Environment

A two dimensional target area of size $m \times n$ was defined in the Stage Robot Simulator. It was also necessary to design a simple model of our robot so that the robot footprint had

the dimensions of the Husky robot presented in figure 1. According to the Clearpath-robotics Husky tech-specs [15], the size of the robot is $0.99\,m \times 0.67\,m$, from a top point of view. The arm dimensions were also designed accordingly, $1\,m$ arm length, the arm sweeping angle was limited to 60° and the angular velocity of the arm was set to $\omega_a = \frac{1}{2}$ rad/s. The velocity commands $(v1, v2, v3, v4, v5)$ sent to this simulated robot are the same as the ones issued for the real robot. The energy consumption was measured during the motion by our polynomial fitting generated models P_{mw} and P_{ma}. Since in the physical robot we use GPS RTK and a very accurate localization is achieved, in the simulator we are using perfect-odometry as the localization reference. In order to simulate the sensors, a bivariate Normal distribution was injected in the map, with the center on the location of each simulated mine, this is detected as the sensor is swept over the area of the mine.

To guaranty practical feasibility, navigation planning was configured to avoid stepping on the mines as the robot detects them. This important factor leads the robot's path to have slights deviations from the coverage algorithm initial plan; consequently also the robot's energy consumption.

5.2 Experiments

Each algorithm was tested several times in four different size squared areas ($m = n = \{2, 10, 20, 30\}\,m^2$), the mines were sparsely distributed keeping at least $\gamma + \frac{\gamma}{2}$ distance between them. The amount of mines ($\mid m/3 \mid$) varied according to the size of the area, the shape of the target area was kept as a square. The size of the mines was kept constant for all tests, this size was selected based on real tests [3] when scanning the M114 (also known as MAPS), an old Portuguese made anti-personal blast mine.

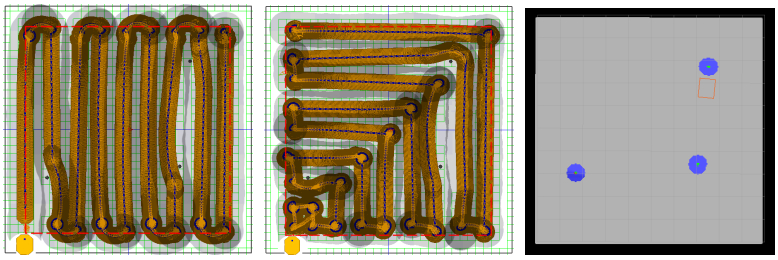

(a) Line Sweep (b) SCD (c) Mines Position

Fig. 7. Trajectory of the robot for both coverage algorithms.

6 Results and discussion

Our study is both theoretical and practical, we formulate a general problem in motion planning and use a skid-steer robot with a sweeping end-effector to experimentally

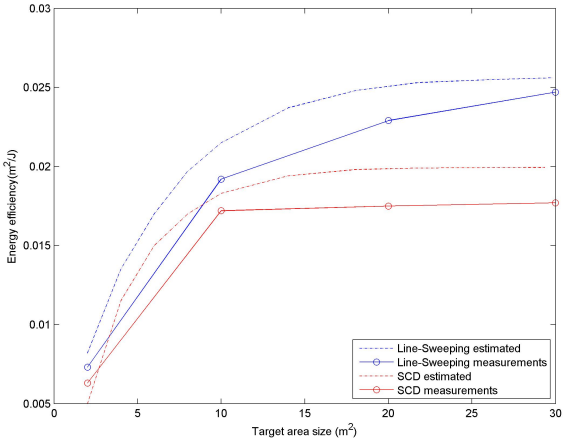

Fig. 8. Energy Efficiency comparison with different target area sizes.

validate our approach. The study presented on section 3, more specifically the relation between the arm sweeping speed and the maximum velocity of the robot, were validated on our robot, but can be easily adapted to any wheeled robot.

Figure 8 shows the estimated and measured energy efficiency of the tested algorithms paths. When the covered area is very small, both algorithms are less efficient because the number of maneuvers are high in relation with the distance traversed in straight lines. As the area increases, both algorithms become better, the Line-Sweeping algorithm was more efficient in all cases. Moreover, as expected, the measurements of the tested scenarios were worst than the estimated efficiency. The reason is that the estimated efficiency was computed for the perfect path of each algorithm, while the measured efficiency uses different accelerations as input, given the slights deviations that the robot has to do in order to avoid stepping on the mines.

Figures 7(b) and 7(a) present trajectory results, where three mines were sparsely positioned in a $10\,m \times 10\,m$ target area. Moreover, since the robot needs to be able to maneuver outside the target area, a $11\,m \times 11\,m$ maneuver space was defined. The robot trail is marked in orange, the sensor trail in light gray and the target area is contoured by a dashed line, the injected bivariate Normal distributions can be seen in Fig. 7(c).

Table 1 presents an additional comparison based on the average of the measurements collected along all the tests, notice that the relations presented in this table are valid for square fields. This study provides a foundation for future research in conserving the energy consumption of wheeled mobile robots. In future work we plan to investigate the behavior of these algorithms in different shapes of target area, and also with a denser set of mines.

Table 1. Additional Comparison

	Line-Sweep	SCD
# of maneuvers	$(2 \cdot m - 1) + deviations$	$(3 \cdot m) + deviations$
Traversed distance	$m^2 - 1 + deviations$	$m^2 - 1 + deviations$
% of overlapping	15%	13%
% of covered area	100%	100%

7 Conclusions

In this paper we analyzed the kinematics of our robot and how it influences the energy consumption during movements. We also defined the power consumption model of the robot's motors, and a relation between the velocity of the arm sweep and the maximum velocity of the robot in order to guaranty a motion scan without any gaps. Moreover we analyzed, tested and compared different coverage algorithms in a simulated environment, also comparing the perfect planned path efficiency with feasible case scenarios for the demming application. In the considered setup, the end-effector motion results from the motion of the platform or the arm, or both. A cost function for these possible end-effector movements was defined and used to evaluate the global cost of covering a given area with different coverage algorithms.

Acknowledgements

This work was partially carried-out in the framework of TIRAMISU project (www.fp7-tiramisu.eu). This project is funded by the European Community's Seventh Framework Program (FP7/SEC/284747).

References

1. S. Larionova, L. Marques, and A. de Almeida, "Toward practical implementation of sensor fusion for a demining robot," in *IEEE/RSJ Int. Conf. on Intelligent Robots and Systems*, 2004.
2. M. Y. Rachkov, L. Marques, and A. T. de Almeida, "Multisensor demining robot," *Autonomous robots*, vol. 18, no. 3, pp. 275–291, 2005.
3. J. Prado, G. Cabrita, and L. Marques, "Bayesian sensor fusion for land-mine detection using a dual-sensor hand-held device," *IECON 2013, the 39th Annual Conference of the IEEE Industrial Electronics Society*, 2013.
4. W. H. Huang, "Optimal line-sweep-based decompositions for coverage algorithms," in *Robotics and Automation, 2001. Proceedings 2001 ICRA. IEEE International Conference on*, vol. 1. IEEE, 2001, pp. 27–32.
5. S.-W. Ryu, Y.-h. Lee, T.-Y. Kuc, S.-H. Ji, and Y.-S. Moon, "A search and coverage algorithm for mobile robot," in *Ubiquitous Robots and Ambient Intelligence (URAI), 2011 8th International Conference on*. IEEE, 2011, pp. 815–821.
6. T.-K. Lee, S.-H. Baek, S.-Y. Oh, and Y.-H. Choi, "Complete coverage algorithm based on linked smooth spiral paths for mobile robots," in *Control Automation Robotics & Vision (ICARCV), 2010 11th International Conference on*. IEEE, 2010, pp. 609–614.

7. E. Gonzalez and E. Gerlein, "BSA-CM: A multi-robot coverage algorithm," in *Web Intelligence and Intelligent Agent Technologies, 2009. WI-IAT'09. IEEE/WIC/ACM International Joint Conferences on*, vol. 2. IET, 2009, pp. 383–386.
8. S. Larionova, N. Almeida, L. Marques, and A. de Almeida, "Olfactory coordinated area coverage," *Autonomous Robots*, vol. 20, no. 3, pp. 251–260, 2006.
9. H. Choset, "Coverage for robotics–a survey of recent results," *Annals of mathematics and artificial intelligence*, vol. 31, no. 1-4, pp. 113–126, 2001.
10. P. Gonzalez de Santos, J. A. Cobano, E. Garcia, J. Estremera, and M. Armada, "A six-legged robot-based system for humanitarian demining missions," *Mechatronics*, vol. 17, no. 8, pp. 417–430, 2007.
11. J. Irwin, M. P. Kazmierkowski, R. Krishnan, and F. Blaabjerg, *Control in power electronics: selected problems*. Book, Elsevier, 2002.
12. J. Tal, "Speed control by phase-locked servo systems–new possibilities and limitations," *Industrial Electronics and Control Instrumentation, IEEE Transactions on*, no. 1, pp. 118–125, 1977.
13. M. Furlan, A. Cernigoj, and M. Boltezar, "A coupled electromagnetic-mechanical-acoustic model of a dc electric motor," *COMPEL: The International Journal for Computation and Mathematics in Electrical and Electronic Engineering*, vol. 22, no. 4, pp. 1155–1165, 2003.
14. A. M. Lewis, T. J. Bloodworth, D. M. Guelle, F. R. Littmann, A. Logreco, and M. A. Pike, "Systematic test & evaluation of metal detectors (STEMD) interim report laboratory tests italy," Institute for the Protection and Security of the Citizen, Tech. Rep., 2006.
15. C. Robotics. Husky tech specs. [Online]. Available: http://www.clearpathrobotics.com/husky/tech-specs/